Generalized Analysis of High-Order Switch-RC N-Path Mixers and Filters using the Adjoint Network

Shanthi Pavan, *Senior Member, IEEE* and Eric Klumperink, *Senior Member, IEEE*

***Abstract*—This paper presents a systematic analysis method for N-path mixers and filters, consisting of periodically switched RC-networks of arbitrary order. It is assumed that each capacitor periodically exchanges charge with the rest of the network during the on-phase of the switching clock, then samples its charge, and holds it perfectly until the next on-phase. This assumption allows for using the adjoint network for simplified analysis of the harmonic transfer functions that describe the signal transfer and folding. Moreover, harmonic transfer cancellations due to the N-path implementation with N equal capacitors switched by N non-overlapping clocks is systematically analyzed. The method is applied to a recently published N-path filter-mixer combination and verified by simulations.**

I. Introduction

The development of integrated, widely tunable, narrow-band, linear, low-noise bandpass filters has been the holy-grail of radio-frequency engineering. As the dynamic range of radios is high, linear filtering is crucial; this is the reason to use only passive components, i.e., mostly R-C circuits (with possibly a few inductors at RF, where they can have reasonable size and quality factor). The traditional approach to bandpass filter design has been to transform a prototype lowpass network using a frequency transformation [1]. The basic idea behind this approach is illustrated using Fig. 1. Part (a) of the figure shows a lowpass passive RC network where the capacitors (the memory elements) are shown explicitly. The impulse response and 3-dB bandwidth of the lowpass filter are denoted by $h_{lp}(t)$ and f_b respectively. The memoryless part of the network is assumed to consist only of resistors. To realize a bandpass transfer function with a center frequency f_s and RF bandwidth f_b, where $f_s \gg f_b$, appropriately chosen inductors are placed in parallel with each of the capacitors, as shown in Fig. 1(b). It can be shown (see for instance, [1]) that the inductance values needed are given by

$$L_m = \frac{1}{4\pi^2 f_s^2 C_m} = \frac{1}{\omega_s^2 C_m}. \tag{1}$$

All the parallel LC tanks in Fig. 1(b) resonate at f_s. Representative frequency responses of the lowpass and bandpass networks are shown in Fig. 1(c). Note that the baseband bandwidth and the RF bandwidth are the same if $f_s \gg f_b$. If f_s is very high, the values of the inductors are small enough that they can be implemented on an integrated circuit. However, apart from being bulky, inductors are lossy, introduce parasitics, and are not tunable.

Another form of the lowpass-to-bandpass transformation becomes possible if we allow the network to become periodically time varying. A passive RC implementation with periodic switching allows for narrow bandwidth, high linearity and low noise.

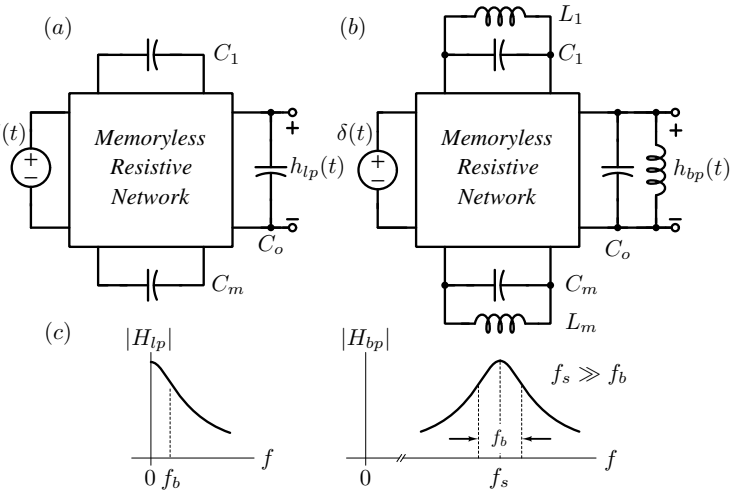

Fig. 1. (a) An RC lowpass network with impulse response $h_{lp}(t)$. (b) Converting it into a bandpass network using the lowpass-to-bandpass transformation. (c) Example magnitude responses of the lowpass and bandpass filters.

As the switching frequency becomes the filter center-frequency, a digitally programmable second-order filter suitable for software defined radio results. This is the approach underlying N-path filters, which have been the subject of intense recent work [2]–[16]. Many of these prior works have analyzed N-path filters in the frequency domain [6]–[8], [17]. The key conclusion is that an N-path bank of switched capacitors behaves like a tuned LC network in the vicinity of the switching frequency. [10] uses this intuition to describe high-order N-path filters. This approach, while being useful, does not predict frequency translation effects from integer multiples of the center frequency.

One of the triggers of this work is the wish to analyze the circuit in [18], which combines N-path filtering and N-path mixing using a second-order switch-RC network. The aim of this work, therefore, is to address high-order switch-RC kernels of arbitrary complexity, where multiple capacitors interact. A systematic approach is necessary to address this complexity. Rather than work in the frequency domain like in prior work (see for instance [2], [10], [13], [15]), we use a time-domain approach that exploits the ideas of reciprocity and the adjoint network, extending and generalizing the work in [16]. A state-space formulation in conjunction with the adjoint-network technique yields the harmonic transfer functions of the system. We are thus able to not only determine the desired transfer function but also the effects of folding from out-of-band frequencies. The expressions we derive are immediately relatable to those derived in the first-order case [2], [13], [16]. The analysis forms the

subject of the rest of the paper, which is organized as follows. In Section II, we first summarize some important properties of sampled LPTV networks central to our work. We then present a first-principles development of an LPTV-network approach to the lowpass-to-bandpass transformation. The passive-mixer and N-path filter modes of operation are discussed. Section III presents a generalized analysis of high-order switch-RC N-path circuits, based on the adjoint approach. The general analysis of such high-order networks using prior methods [2], [13], [19], [20] is bound to be algebraically involved. We leverage our recent work on the unified analysis of the first-order switched-RC network [16] along with state-space methods. Thanks to this, the results we obtain are in the same simple form obtained for the first-order switched-RC network. In Section IV, we give the signal-flow graph for the complete output waveforms in switch-RC N-path networks, and simplified graphs for operation in the passive-mixer and N-path filter modes. Section V applies the theory developed in this paper to a recently reported 4-path mixer-first receiver [18]. We show that the network can be derived from a prototype second-order lowpass RC filter. We then apply our theory to derive expressions for the mixer's conversion gain. Conclusions are given in Section VI.

II. Evolution of Switched-RC N-Path Filters

Fig. 2(a) shows an LPTV network. The switch is periodically operated at a frequency f_s. Determining the complete output $v_o(t)$ for an arbitrary input is difficult, since the evaluation of tedious convolution integrals is involved (even for this simple circuit). Suppose, however, that we are only interested in determining one sample of the output per period; namely $v_o(lT_s)$ (l is an integer). Determining the complete output first and then sampling it is inefficient, as we first solve tedious integral equations to find the full waveform and then throw away most of that information. It seems reasonable that a simpler technique can be found. This is where the properties of sampled LPTV networks [21] come in handy. We summarize them below, using the network of Fig. 2(a) as an example.

The switched-RC network of Fig. 2(a) is an LPTV network varying at a frequency f_s and is excited by a voltage input $v_i(t)$. The output is the capacitor voltage $v_o(t)$.

a. The sampled sequence $v_o(lT_s)$ can be thought of as being obtained by sampling the output of an appropriately chosen linear *time-invariant* (LTI) system excited by $v_i(t)$. The LTI filter's impulse response is denoted by $h_{eq}(t)$.
b. $h_{eq}(t)$ can be determined using the adjoint network, as elaborated below.

The adjoint network is derived using the following rules.

1. A resistive or capacitive branch in the original network remains unchanged in the adjoint.
2. A periodically operated switch in the original network, controlled by a waveform $\phi(t)$, is replaced in the adjoint by a switch that is controlled by $\phi(-t)$.

The adjoint of the network of Fig. 2(a) is shown in part (b) of the figure. To find $h_{eq}(t)$, a *current* impulse excites the output node of the adjoint network, and the current $i_{out}(t) = h_{eq}(t)$ in the input branch is recorded.

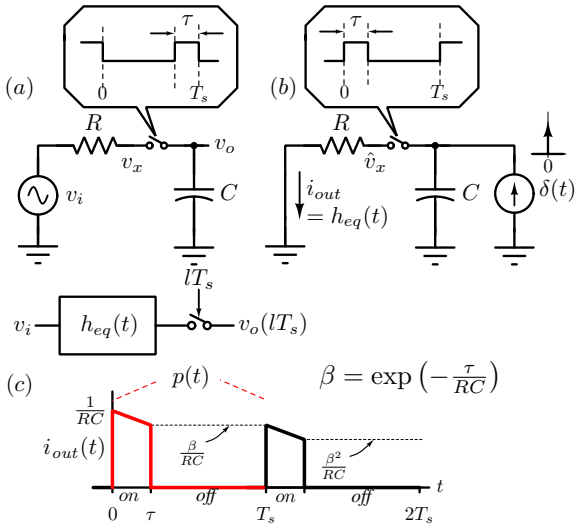

Fig. 2. (a) Original network. The output $v_o(t)$ sampled at $t = lT_s$, where l is an integer, is of interest. (b) Determining the impulse response of the equivalent LTI filter using the adjoint network. (c) $i_{out}(t) = h_{eq}(t)$ waveform.

Why is the adjoint-network technique simple to use? In this method, we excite the network at the output *only once* (as opposed to a sinusoidal excitation on the original network as in prior work that uses frequency-domain analysis [2], [13]), at a moment that corresponds to the sampling instant (after the time-reversal action). In Fig. 2(b), this corresponds to injecting a current impulse across C at $t = 0$ (since the output is being sampled at lT_s). The resulting current during the first time period ($0 \le t < T_s$), which we denote by $p(t)$, provides all the necessary information that we are after. This is due to the following. The adjoint network, being periodically time-varying, essentially responds in the same way in subsequent time-periods, except for a difference in its initial conditions. Referring to Fig. 2(b) and (c), i_{out}, which is initially $1/RC$, decays with a time-constant RC for a duration τ, and is zero for the rest of the period. At $t = T_s+$, the capacitor voltage is $\beta = \exp(-\tau/RC)$ times the voltage at $t = 0+$. It must thus follow that i_{out} in the second period must be $\beta p(t-T_s)$. It is thus possible to determine $h_{eq}(t)$ from the adjoint network using recursion [16], [22]. In Fig. 2(b), it is seen that $i_{out}(t) = h_{eq}(t)$ is given by the recursive relation

$$h_{eq}(t) = p(t) + \beta h_{eq}(t - T_s), \tag{2}$$

which in the frequency domain is expressed as

$$H_{eq}(f) = \frac{P(f)}{1 - \beta e^{-j2\pi f T_s}}. \tag{3}$$

From the discussion above, we see that the adjoint impulse-response technique enables us to determine the sampled output of the LPTV system in a simple manner. Fortunately, in the class of circuits analyzed in this paper (which also happen to be of practical importance), the sampled outputs play a central role in determining the various transfer functions of interest. As seen in the rest of the paper, the use of the adjoint network also greatly simplifies the analysis of high-order switched-RC networks. State-space techniques are used to derive compact relations for various transfer functions. These relations are im-

mediately relatable to those obtained in [2], [13], [16] in the first-order example of Fig. 2(a).

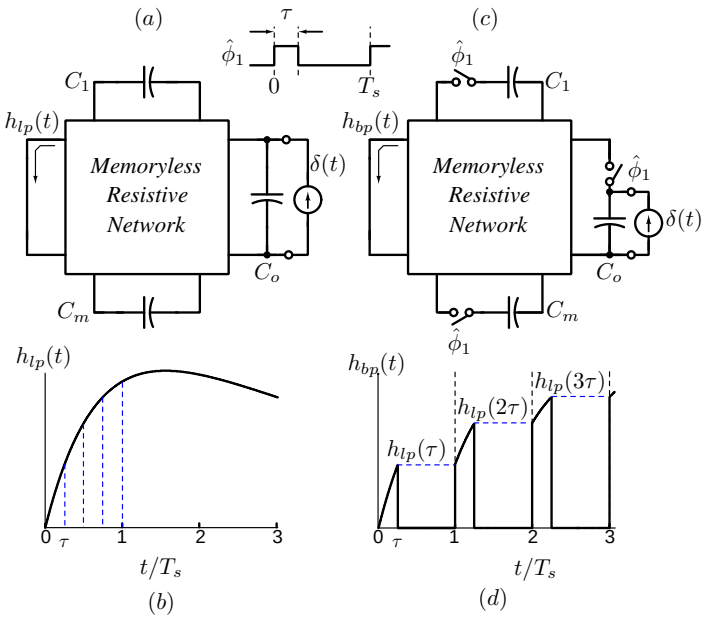

Fig. 3. (a) The lowpass network of Fig. 1(a) excited by an impulse current at its output port. (b) The current in the input port. (c) A switch, controlled by $\hat{\phi}_1$, is inserted in series with every capacitor, resulting in an LPTV system. (d) Impulse response of the equivalent LTI filter relating the input to the sampled output of the adjoint of the LPTV network.

Consider again our high-order RC lowpass network of Fig. 1(a), with an impulse response $h_{lp}(t)$. By reciprocity, the same impulse response is obtained at the input port by exciting the output port with an impulse current, as shown in Fig. 3(a). An example impulse response $h_{lp}(t)$ is shown in part (b) of the figure. Let us now examine the network of Fig. 3(c), which is the same as that of Fig. 3(a), except that every capacitor has in series with it a periodically operated switch, controlled by the waveform $\hat{\phi}_1$. The resulting network is now an LPTV one. $\delta(t)$ is injected into the output port. The resulting current waveform in the input port is denoted by $h_{bp}(t)$. One might wonder how is $h_{bp}(t)$ related to $h_{lp}(t)$.

For $0 \leq t < \tau$, the switches are closed; in this interval, therefore, $h_{bp}(t) = h_{lp}(t)$. At $t = \tau$, the switches are opened. Since all the sources of charge are now isolated from the resistive network, the currents in all the network branches are zero. Thus, $h_{bp}(t) = 0$ for $\tau \leq t < T_s$. Further, all capacitor voltages are "frozen" due to the hold operation until the switches turn on again at $t = T_s$. At this juncture, the network resumes from "where it left off"; so $h_{bp}(T_s) = h_{lp}(\tau)$, as shown in Fig. 3(b). In the time interval $T_s \leq t < T_s + \tau$, $h_{bp}(t) = h_{lp}(\tau + (t - T_s))$. In general, it is easy to see that

$$h_{bp}(lT_s + t_1) = \begin{cases} h_{lp}(l\tau + t_1), & \text{for } 0 \leq t_1 < \tau \\ 0, & \text{for } \tau \leq t_1 < T_s \end{cases}$$

where l is an integer. Moreover, since the capacitors hold their state when the switches are off, it follows that

$$h_{bp}(lT_s+) = h_{lp}(l\tau). \tag{4}$$

In practice, $h_{lp}(t)$ "lasts" for many clock periods, since the bandwidth of the lowpass transfer function is much smaller than f_s. Thus, from the discussion above, and Figs. 3(b) and (d), it is apparent that the envelop of $h_{bp}(t)$ is approximately a time-stretched version of $h_{lp}(t)$, as shown in Fig. 4(a)[1]. Such filters have also been studied as "stop-go" N-path filters in the literature [20], [23], [24]. However, those approaches either use multidimensional time or frequency domain methods.

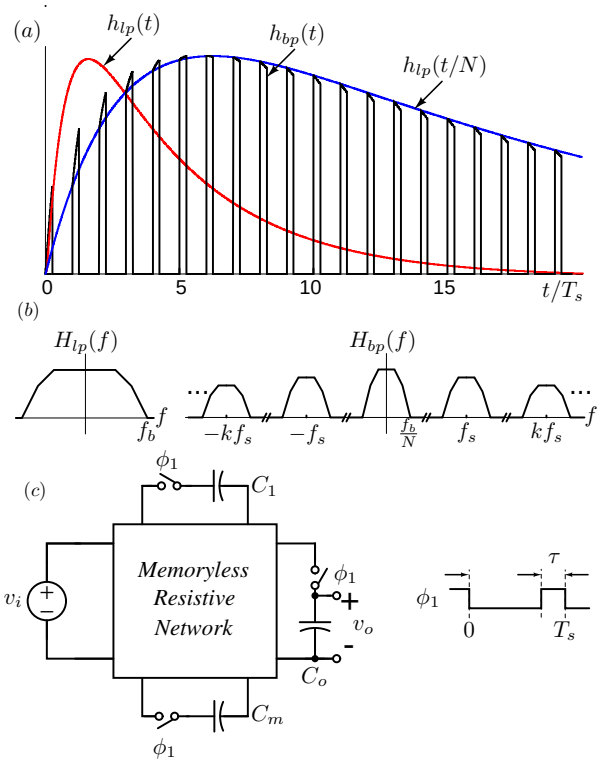

Fig. 4. (a) Comparison of $h_{lp}(t)$, $h_{lp}(t/N)$ and $h_{bp}(t)$. (b) Example magnitude responses $|H_{lp}(f)|$ and $|H_{bp}(f)|$. (c) Network of Fig. 3(c), with the locations of the excitation and response interchanged.

$h_{bp}(t)$ may be interpreted as the product of a rectangular pulse train $\hat{w}(t)$ with period T_s and duty cycle τ/T_s, and $h_{lp}(t/N)$. We have

$$h_{bp}(t) \approx h_{lp}(t/N) \cdot \hat{w}(t) \tag{5}$$

where

$$\hat{w}(t) = \begin{cases} 1, & \text{for } lT_s \leq t < lT_s + \tau \\ 0, & \text{otherwise} \end{cases} \tag{6}$$

Since multiplication by $\hat{w}(t)$ in the time domain corresponds to convolution in the frequency domain, we have

$$H_{bp}(f) \approx N \sum_{k=-\infty}^{\infty} a_k H_{lp}\left((f - kf_s)N\right) \tag{7}$$

where the a_k are the coefficients of the Fourier expansion of $\hat{w}(t)$. As (7) shows, $H_{bp}(f)$ is related to $H_{lp}(f)$ as follows:

[1]The astute reader would have noticed the significant deviation between the envelop of $h_{bp}(t)$ and $h_{lp}(t/N)$ for small t. This is because the ratio of the bandwidth of the lowpass network to f_s is not very small in Fig. 4 (for clarity). In practice, $h_{lp}(t)$ will be much slower, greatly reducing the difference between the two.

a. H_{lp} is frequency shifted to around multiples of kf_s.
b. The "offset frequency" $(f - kf_s)$ is scaled by a factor $1/N$.

As shown in Fig. 4(b), $H_{bp}(f)$ has passbands at multiples of f_s. The shape of each passband mimics that of the lowpass prototype whose frequency response has been frequency-scaled by $1/N$. Although this is some form of lowpass to bandpass conversion, note that the RF bandwidth is not equal to the baseband bandwidth, but is scaled by a factor $1/N$. This makes intuitive sense – since the capacitors are "in contact" with the resistors with a duty-cycle of $1/N$, they will take N-times more time to be discharged.

Consider now the network of Fig. 4(c), which is the same as the network of Fig. 3(c), except that the control signals of the switches are time-reversed, and the locations of the excitation and response interchanged. The reader will immediately recognize that the networks of Fig. 4(c) and Fig. 3(c) are adjoints of each other. From the properties of sampled LPTV networks and the adjoint discussed earlier in this section, it must follow that the impulse response of the equivalent LTI filter relating the input voltage v_i in Fig. 4(c) to the sampled output ($v_o[lT_s]$) is given by $h_{bp}(t)$ of Fig. 3(d), which in the frequency domain corresponds to a response that has multiple passbands as shown in Fig. 4(d). There are several possibilities of "tapping" the output voltage, as described below.

A. Passive-Mixer Mode:

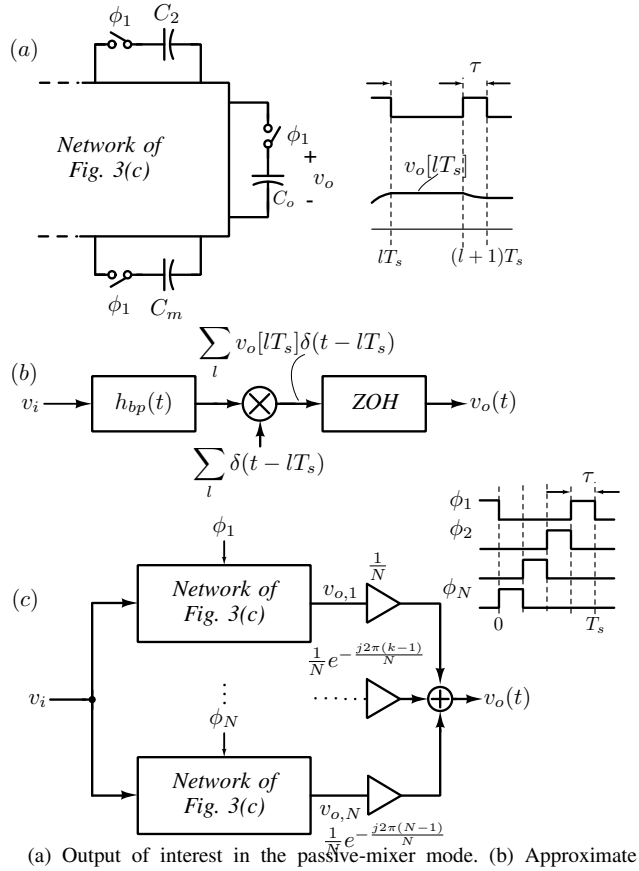

Fig. 5. (a) Output of interest in the passive-mixer mode. (b) Approximate equivalent circuit. (b) Using N paths to address folding from harmonics of f_s. ($N = 4$ in this example).

In this mode of operation, the *entire* voltage waveform across the capacitor C_o in Fig. 4(c) is of interest. As shown in Fig. 5(a), $v_o[lT_s]$, which is the voltage sampled on C_o at the falling edge of ϕ_1 in the l^{th} clock cycle, is held for a duration $(T_s - \tau)$ (from $lT_s \le t < (l+1)T_s - \tau$), since C_o is effectively disconnected from the network. When ϕ_1 goes high again at $t = (l+1)T_s - \tau$, C_o (dis)charges slowly, since the time-constants are much larger than T_s. Thus, the continuous-time waveform $v_o(t)$ can be thought of as being the zero-order-hold (ZOH) version of $v_o[lT_s]$.

The approximate block diagram relating $v_i(t)$ to $v_o(t)$ is shown in Fig. 5(b). The RF input is first filtered by a continuous-time bandpass filter with impulse response $h_{bp}(t)$, and sampled by multiplying with a periodic Dirac impulse train. The resulting modulated impulse train excites a ZOH that holds for a complete clock period. Since the ZOH is a lowpass operation with transmission zeros at multiples of f_s, the output $v_o(t)$ can be thought of as being a lowpass filtered version of the impulse sequence $\sum_l v[lT_s]\delta(t - lT_s)$. Thus, the circuit of Fig. 4(c) can be thought of as a receiver with down-conversion mixing. The names "mixing region" [2] and "passive-mixer" mode [13] are thus justified. The passband-locations of the RF bandpass filter are accurately set by the clock frequency, and are easily tunable. The shape of the passband is determined by the frequency response of the lowpass prototype. This way, precise control of the center frequency and independent control of the bandwidth and shape are obtained. Unfortunately, however, the bandpass filter has passbands around all integer multiples of f_s, while the desired input signal is centered around f_s. This can be problematic, as described below.

The k^{th} harmonic transfer function of this system of Fig. 5(a), which quantifies the gain from an input frequency f to an output frequency $(f + kf_s)$ can be calculated as follows. When $v_i = e^{j2\pi ft}$, the sampled output sequence is given by

$$v_o[lT_s] = H_{bp}(f)e^{j2\pi flT_s}. \tag{8}$$

$v_o(t)$ is the ZOH version of $v_o[lT_s]$. $H_k(f)$ is thus seen to be

$$H_k(f) = H_{bp}(f)\,\mathrm{sinc}((f + kf_s)T_s) \tag{9}$$

where sinc refers to the normalized function $\mathrm{sinc}(x) = \sin(\pi x)/(\pi x)$. Let $v_i(t)$ consist of a desired tone at f_s with amplitude A_1 and an interfering tone at $2f_s$ with amplitude A_2. The output of the passive mixer will be $A_1H_{-1}(f_s) + A_2H_{-2}(2f_s) = A_1H_{bp}(f_s) + A_2H_{bp}(2f_s)$. Since the bandpass filter has passbands around integer multiples of f_s, $|H_{bp}(f_s)|$ and $|H_{bp}(2f_s)|$ are comparable, indicating that interferers from $2f_s$ are demodulated to baseband with very little attenuation. Reasoning in a similar manner, we conclude that unwanted signals around integer multiples of f_s are downconverted to low frequency. This can be avoided by using N-path techniques, as described below.

Consider the system of Fig. 5(c), where v_i excites N instances of the network of Fig. 4(c), except that the switches are controlled by clocks $\phi_1, \phi_2, \cdots, \phi_N$, each advanced in time by $\tau = T_s/N$ with respect to the other. The harmonic transfer functions when the switches are controlled by ϕ_1 are denoted by

H_k. Thus, in Fig. 5(c), with $v_i(t) = e^{j2\pi ft}$,

$$v_{o,1}(t) = \sum_k H_k(f) e^{j2\pi(f+kf_s)t}. \quad (10)$$

When the timing control signal is advanced by $\tau = T_s/N$, the harmonic transfer functions are $H_k e^{j2\pi k/N}$. Referring to Fig. 5(c) we have

$$\begin{aligned} v_{o,2}(t) &= \sum_k e^{\frac{j2\pi}{N}k} H_k(f) e^{j2\pi(f+kf_s)t} \\ \vdots &= \vdots \\ v_{o,n}(t) &= \sum_k e^{\frac{j2\pi}{N}(n-1)k} H_k(f) e^{j2\pi(f+kf_s)t}. \quad (11) \end{aligned}$$

Weighted addition of $v_{o,1}, \cdots, v_{o,N}$ by the complex coefficients $1/N, (1/N)e^{-\frac{j2\pi}{N}}, \cdots, (1/N)e^{-\frac{j2\pi(N-1)}{N}}$ yields the complex baseband signal

$$\begin{aligned} v_o(t) &= \frac{1}{N}\left(v_{o,1}(t) + e^{-\frac{j2\pi}{N}} v_{o,2}(t) + \cdots + e^{-\frac{j2\pi(N-1)}{N}} v_{o,N}(t)\right) \\ &= \cdots + H_{-1}(f) e^{j2\pi(f-f_s)t} + H_{-(N+1)}(f) e^{j2\pi(f-(N+1)f_s)t} + \cdots \end{aligned}$$

From the equation above, we see that weighted addition of the outputs of N paths eliminates downconversion from frequencies of the form $f + 2f_s, f + 3f_s, \cdots, f + Nf_s$ etc. Even though the system of Fig. 5(c) is LPTV with a frequency f_s, many of the harmonic transfer functions from v_i to $v_o(t)$ are zero since the contributions from the N paths cancel. Thus, Fig. 5(c) represents a downconversion mixer that has a bandpass filter up-front, whose passbands are centered around $f_s, (N+1)f_s, \cdots, (2N+1)f_s$ etc. (as opposed to $f_s, 2f_s, 3f_s, \cdots$ etc. for the system of Fig. 5(a)). Thanks to N-path operation, a simple passive filter that rejects interferers around $(N+1)f_s$ is all that is needed to prevent spurious tones from being downconverted to baseband.

B. N-path Filter Mode:

An alternative way of operation is the N-path filter mode, whose basic idea is described using Fig. 6. Part (a) of the figure shows the network of Fig. 4(c). The voltage across C_o, namely $v_o(t)$, is conceptually multiplied by the clock waveform ϕ_1, yielding an output voltage $v_o(t) \cdot \phi_1$, that is nonzero only when $(l+1)T_s - \tau \le t < (l+1)T_s$. As in the passive-mixer case, the voltage held on the capacitor at the falling edge of ϕ_1 plays a key role in the output waveform. Since network time-constants are much larger than T_s, the output during the lth clock cycle can be (approximately) thought of as holding $v_o(lT_s)$ for a duration τ and delaying the result by $(T_s - \tau)$. The approximate model relating $v_i(t)$ to $v_o(t) \cdot \phi_1$ is thus given by Fig. 6(b). When $v_i(t) = e^{j2\pi ft}$, $v_o(t) \cdot \phi_1$ consists of components whose frequencies are of the form $f + kf_s$ (due to LPTV operation).

$$v_o(t) = \sum_k H_k(f) e^{j2\pi(f+kf_s)t}. \quad (12)$$

Analysis of Fig. 6(b) shows that

$$|H_k(f)| = \frac{1}{N}\left| H_{bp}(f) \mathrm{sinc}\left(\frac{(f+kf_s)T_s}{N}\right)\right|. \quad (13)$$

From the equation above, and recalling that $H_{bp}(f)$ has passbands around integer multiples of f_s, we see that spurious inputs around

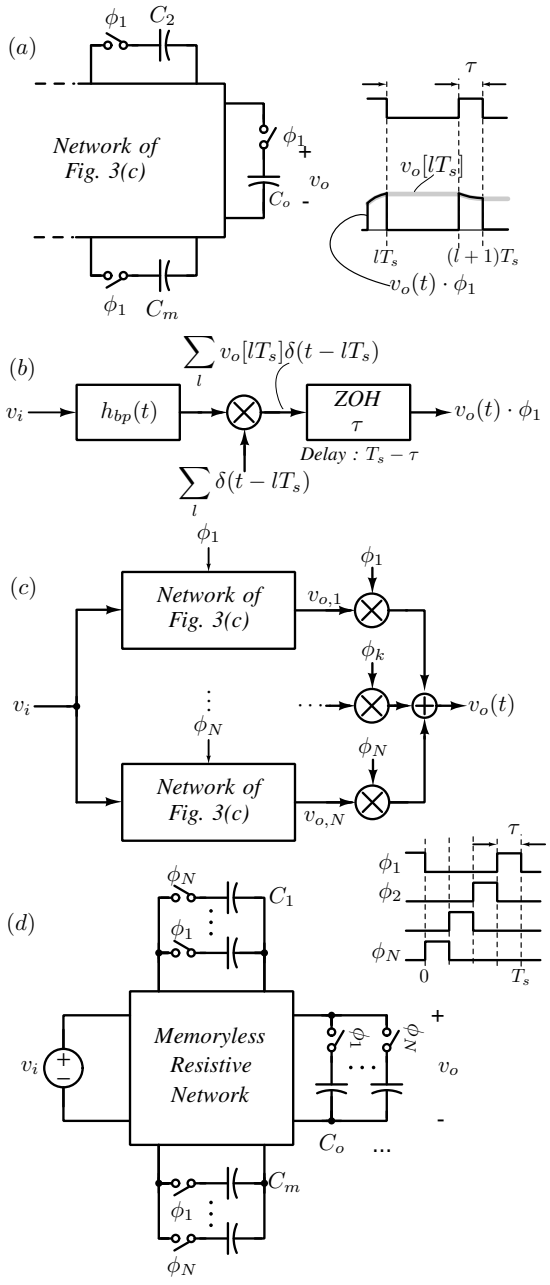

Fig. 6. (a) The relevant output for the N-path filter mode is $v_o(t) \cdot \phi_1$. (b) Approximate equivalent signal-flow diagram. (c) Operating N switched circuits with phase-shifted clocks to obtain N-path filtering. Adding $v_{o,1}, \cdots, v_{o,N}$ results in harmonic rejection. (d) Equivalent realization of the N instances of the lowpass prototype in Figs. 5(c) and part (c) of this figure.

kf_s could get translated to f_s at the filter output. As in the passive-mixer mode, this can be largely addressed using an N-path structure, as shown in Fig. 6(c). N copies of the networks of the type in Fig. 4(c) are operated with phase-shifted clocks $\phi_1, \cdots, \phi_N$ and their their outputs are multiplied by $\phi_1, \cdots, \phi_N$ respectively. The outputs are then added to yield $v_o(t)$. Analysis of Fig. 6(c) indicates that only harmonic transfer functions whose order is an integer multiple of N are non-zero; those of other orders are canceled due to N-path operation. Thus, a gentle filter can be used upfront to eliminate spurious tones that would otherwise alias on to the desired frequency f. Thus, the N-

path structure of Fig. 6(c) represents a tunable narrow-band filter without the use of inductors.

Observing Figs. 5(c) and 6(c), we see that both systems are essentially N copies of the switched lowpass prototype; and appropriately-weighted addition of the voltages across C_o yield the final output. Referring to the network of Fig. 4(c), we see that the resistive part is essentially idle when the switches are off. Since $\phi_1, \cdots, \phi_N$ do not overlap, the resistive network can be shared by the N copies [23] – the result is shown in Fig. 6(d).

III. Generalized Analysis of N-Path Circuits

In the previous section, we gave an intuitive development of switched-RC N-path circuits. While the intuition is important, it is just as crucial to develop a systematic method of analysis. This is addressed below, and the sections to follow.

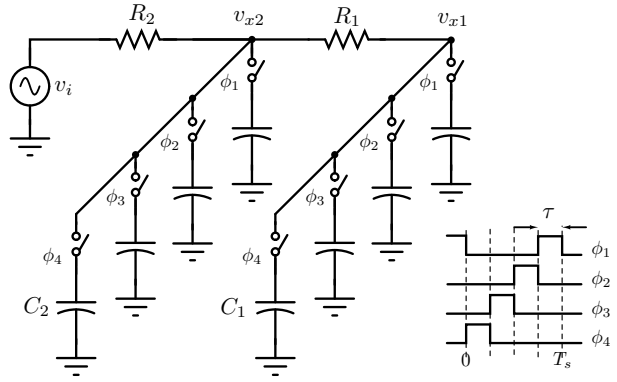

Fig. 7. The switched 4-path example, based on a second order prototype kernel.

We will develop our analysis using a 4-path switched network shown in Fig. 7. The choice of this example circuit does not lead to any loss of generality – while it is sufficiently simple to explain the steps of our analysis, it is not so simple as to be trivial. Observing Fig. 7, we see that while the individual capacitors within each bank (C_1 and C_2) do not interact, that particular set of capacitors in the banks C_1 and C_2 switched on during the same phase are coupled through R_1. Thus, the switched N-path network can be analyzed using the "independent-kernel" approach.

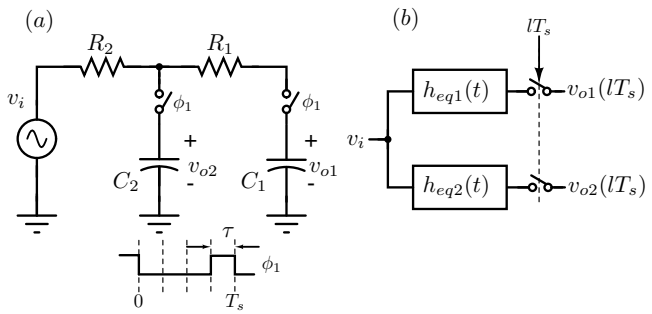

Fig. 8. The kernel corresponding to the network of Fig. 7. (b) Equivalent system relating the input to the sampled outputs.

Fig. 8 shows the kernel corresponding to the network of Fig. 7. Once the kernel's harmonic transfer functions have been evaluated, rotational symmetry can be used to determine the corresponding transfer functions for the N-path structures (mixer and filter). The voltage waveforms across C_1 and C_2 are denoted by $v_{o1}(t)$ and $v_{o2}(t)$ respectively. We denote by $\mathbf{v_o}(t)$ the column vector of capacitor voltages, as shown below.

$$\mathbf{v_o}(t) = \begin{bmatrix} v_{o1}(t) \\ v_{o2}(t) \end{bmatrix}. \tag{14}$$

For a general kernel with m states, $\mathbf{v_o}(t)$ will be an m-dimensional vector. We are interested in determining $\mathbf{v_o}(t)$, which can be separated into two parts; $\mathbf{v_{off}}(t)$ which occurs when the switches are off, and $\mathbf{v_{on}}(t)$, when the switches are turned on. When the switches are off, the capacitors simply hold their states. To determine $\mathbf{v_{off}}(t)$, therefore, we would like to know the voltages sampled on the capacitors at the falling edges of the clock waveform (i.e., at $\mathbf{v_o}(lT_s)$).

The kernel is an LPTV network varying at a frequency f_s. We are interested in determining $\mathbf{v_o}(lT_s)$, which contains all capacitor voltages sampled at the same frequency at which the network is varying. From [21], we know that $\mathbf{v_o}(lT_s)$ can be thought of as being the sampled outputs of linear time-invariant (LTI) filters, driven by $v_i(t)$, as shown in Fig. 8(b). The vector of impulse responses is denoted by $\mathbf{h_{eq}}(t)$. Thus,

$$\mathbf{h_{eq}}(t) = \begin{bmatrix} h_{eq1}(t) \\ h_{eq2}(t) \end{bmatrix}. \tag{15}$$

In the general case (with m state variables), $\mathbf{h_{eq}}(t)$ will be an m-dimensional vector. [21] shows that $\mathbf{h_{eq}}(t)$, can be readily obtained from the adjoint (or inter-reciprocal) network. The adjoint network used to determine $h_{eq1}(t)$ is shown in Fig. 9(a). Note that the switch-control signals in the original network are reversed in time in the adjoint. The voltages in the original LPTV network are sampled at zero timing-offset from lT_s, meaning that we are interested in $\mathbf{v_o}(t)$ at $(lT_s{+}0)$. Thus, to determine $h_{eq1}(t)$, the "output" port of the adjoint is excited by an impulsive current at $t = 0$, and the current waveform through the input port is recorded.

Referring to Fig. 9(c), the current impulse causes $v_1(0+) = 1/{C_1}^2$. $v_2(0+)$, on the other hand is zero. For $0 < t < \tau$, C_1 discharges through the rest of the network. During this process, C_2 gets charged, as shown in Fig. 9(d). $i_{out}(t)$ during this interval, is given by $(1/R_2)v_2(t)$. When the switches are opened at $t = \tau$, the charge on the capacitors is trapped; as a result, v_1 and v_2 do not change during the time-interval $\tau \le t < T_s$. Thus, during $\tau \le t < T_s$, $v_1(t) = v_1(\tau-)$ and $v_2(t) = v_2(\tau-)$. Further, since the switches are open, $i_{out} = h_{eq1}(t) = 0$. We denote i_{out} for $0 \le t < T_s$ by $p_1(t)$, as shown in red in Fig. 9(b).

How are $v_1(\tau-)$ and $v_2(\tau-)$ related to $v_1(0+)$ and $v_2(0+)$? We denote the capacitor voltages v_1 and v_2 in the adjoint by

$$\mathbf{v}(t) = \begin{bmatrix} v_1(t) \\ v_2(t) \end{bmatrix}. \tag{16}$$

When the switches are closed, the network is linear and time-invariant and can be described using the state-space form. With

[2]Throughout this paper, $t-$ and $t+$ denote the time instants just before and just after t respectively. The $1/C_1$ actually has dimensions of voltage, since the 1 stands for 1 Coulomb.

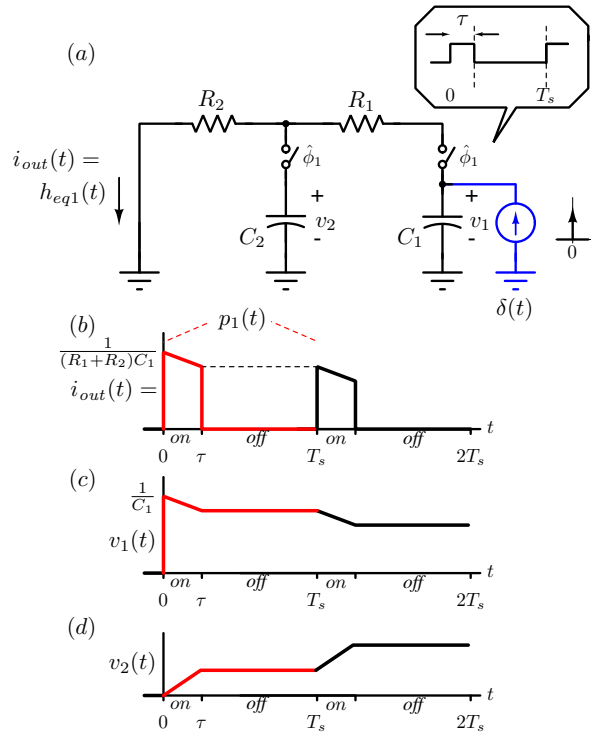

Fig. 9. (a) The adjoint network corresponding to the kernel of Fig. 8. (b) $h_{eq1}(t) = i_{out}(t)$ (c) $v_1(t)$ (d) $v_2(t)$.

a zero input, the capacitor voltages evolve [25] according to $\dot{\mathbf{v}} = \mathbf{A}\mathbf{v}$, where $\mathbf{A}$ denotes the "A"-matrix of the state-space representation. Thus,

$$\mathbf{v}(\tau-) = e^{\mathbf{A}\tau}\mathbf{v}(0+). \tag{17}$$

Since only one output is excited, only the corresponding row of $\mathbf{v}(0+)$ contains a non-zero value. In our example, $\mathbf{v}(\tau-)$ is simply the first column of $e^{\mathbf{A}\tau}$, scaled by $1/C_1$.

At $t = T_s+$, the switches are closed again, and C_1 and C_2 continue to discharge, with initial conditions $v_1(\tau-)$ and $v_2(\tau-)$ respectively. Note that $h_{eq1}(t) = i_{out}(t)$ is the response to a voltage $(1/C_1)$ on C_1 at $t = 0+$, with $v_2(0+) = 0$. Similarly, $h_{eq2}(t)$ is the response to a voltage $(1/C_2)$ on C_2 at $t = 0+$, with $v_1(0+) = 0$. After the first cycle, both capacitors contain charge, and the response to capacitor voltages $v_1(\tau-)$ and $v_2(\tau-)$ at $t = T_s+$ is $\frac{v_1(\tau-)}{1/C_1}h_{eq1}(t-T_s) + \frac{v_2(\tau-)}{1/C_2}h_{eq2}(t-T_s)$. This is a consequence of linearity and the periodically time-varying nature of the network. Thus, $i_{out}(t) = h_{eq1}(t)$ can be expressed as

$$h_{eq1}(t) = p_1(t) + \frac{v_1(\tau-)}{1/C_1}h_{eq1}(t-T_s) + \frac{v_2(\tau-)}{1/C_2}h_{eq2}(t-T_s). \tag{18}$$

Using (17) and $v_1(0+) = 1/C_1$, the equation above can be written as

$$h_{eq1}(t) = p_1(t) + \begin{bmatrix}\frac{1}{C_1} & 0\end{bmatrix} e^{\mathbf{A}^T\tau}\begin{bmatrix}C_1 & 0\\ 0 & C_2\end{bmatrix}\mathbf{h_{eq}}(t-T_s). \tag{19}$$

To determine $h_{eq2}(t)$, a current impulse should be injected across C_2 in the adjoint network of Fig. 9(a), and the resulting i_{out} has to be determined. Proceeding along lines similar to the determination of $h_{eq1}(t)$, we obtain

$$h_{eq2}(t) = p_2(t) + \begin{bmatrix}0 & \frac{1}{C_2}\end{bmatrix} e^{\mathbf{A}^T\tau}\begin{bmatrix}C_1 & 0\\ 0 & C_2\end{bmatrix}\mathbf{h_{eq}}(t-T_s). \tag{20}$$

Combining (19) and (20), we have

$$\mathbf{h_{eq}}(t) = \mathbf{p}(t) + \underbrace{\begin{bmatrix}\frac{1}{C_1} & 0\\ 0 & \frac{1}{C_2}\end{bmatrix} e^{\mathbf{A}^T\tau}\begin{bmatrix}C_1 & 0\\ 0 & C_2\end{bmatrix}}_{e^{\mathbf{A}\tau}}\mathbf{h_{eq}}(t-T_s). \tag{21}$$

It turns out, as shown in Appendix A, that the term atop the brace in (21) reduces to $e^{\mathbf{A}\tau}$. Thus,

$$\mathbf{h_{eq}}(t) = \mathbf{p}(t) + e^{\mathbf{A}\tau}\mathbf{h_{eq}}(t-T_s). \tag{22}$$

Applying the Fourier transform to both sides of (22) yields

$$\mathbf{H_{eq}}(f) = (\mathbf{I} - e^{\mathbf{A}\tau}e^{-j2\pi fT_s})^{-1}\mathbf{P}(f). \tag{23}$$

Note that the equation above is of the same form as (3).

A. *Determining* $\mathbf{p}(t)$

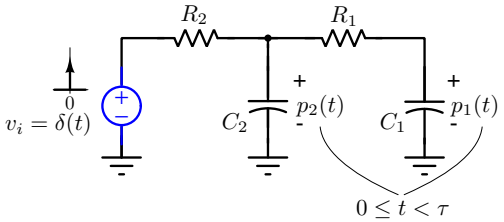

Fig. 10. Network used to determine $\mathbf{p}(t)$ for the time interval $0 < t < \tau$ using reciprocity in the passive network when ϕ_1 is high.

Earlier in this section, $p_1(t)$ and $p_2(t)$ were determined by injecting current impulses into C_1 and C_2 respectively, when the switches were on. This necessitated two evaluations of the adjoint network of Fig. 9 in the time interval $0 \le t < \tau$, i.e., when the switches were closed. During this time interval, the network is linear and time-invariant. This means that rather than evaluating $p_1(t)$ and $p_2(t)$ separately, they can be obtained in one shot invoking reciprocity [26]. As shown in Fig. 10, both the components of $\mathbf{p}(t)$ can be found to be the voltage waveforms across C_1 and C_2 respectively, in the time interval $0 \le t < \tau$, when the network is excited with a voltage impulse.

The capacitor voltages are related to v_i as $\dot{\mathbf{v}} = \mathbf{A}\mathbf{v} + \mathbf{B}v_i$. $\mathbf{p}(t)$ can be written as the difference between two decaying exponentials as follows. For $0 \le t < \tau$, $\mathbf{p}(t) = e^{\mathbf{A}t}\mathbf{B}u(t)$, where $u(t)$ denotes the unit-step function. At $t = \tau$, the capacitor voltages will be $e^{\mathbf{A}\tau}\mathbf{B}u(t)$, and for $t > \tau$, would evolve as $e^{\mathbf{A}(t-\tau)}e^{\mathbf{A}\tau}\mathbf{B}u(t-\tau)$. $\mathbf{p}(t)$, therefore, can be expressed as

$$\mathbf{p}(t) = e^{\mathbf{A}t}\mathbf{B}u(t) - e^{\mathbf{A}\tau}e^{\mathbf{A}(t-\tau)}\mathbf{B}u(t-\tau). \tag{24}$$

In the frequency domain, this corresponds to

$$\mathbf{P}(f) = \left(\mathbf{I} - e^{\mathbf{A}\tau}e^{-j2\pi f\tau}\right)(j2\pi f\mathbf{I} - \mathbf{A})^{-1}\mathbf{B}. \tag{25}$$

Combining (23) and (25), we have the following expression for $\mathbf{H_{eq}}(f)$.

$$\mathbf{H_{eq}}(f) = \tag{26}$$
$$(\mathbf{I} - \mathbf{e}^{\mathbf{A}\tau}e^{-j2\pi fT_s})^{-1}\left(\mathbf{I} - \mathbf{e}^{\mathbf{A}\tau}e^{-j2\pi f\tau}\right)(j2\pi f\mathbf{I} - \mathbf{A})^{-1}\mathbf{B}.$$

It is instructive to observe the form taken by (26) for the special case of the switched-RC N-path filter. In this case, the kernel is a first-order system, with $\mathbf{A} = -1/RC$, $\mathbf{B} = 1/RC$, and $e^{\mathbf{A}\tau} = e^{-\tau/RC}$. Denoting $e^{-\tau/RC} \equiv \beta$, we obtain

$$H_{eq}(f) = \underbrace{\frac{1}{1-\beta e^{-j2\pi f T_s}}}_{(\mathbf{I}-e^{\mathbf{A}\tau}e^{-j2\pi f T_s})^{-1}} \overbrace{(1-\beta e^{-j2\pi f\tau})}^{\mathbf{I}-\mathbf{e}^{\mathbf{A}\tau}e^{-j2\pi f\tau}} \underbrace{\frac{1}{(1+j2\pi fRC)}}_{(j2\pi f\mathbf{I}-\mathbf{A})^{-1}\mathbf{B}}$$

which is identical to the results obtained in [2], [13], and [16].

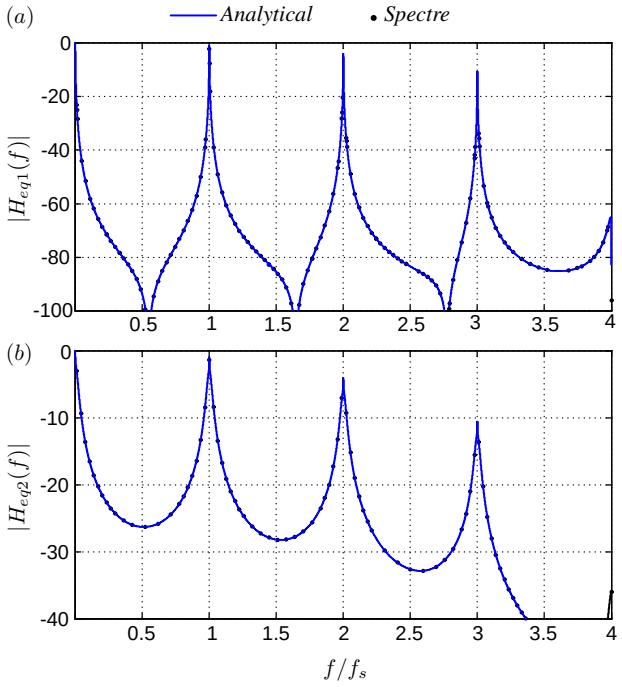

Fig. 11. Comparison of (26) and simulations of $|H_{eq1}(f)|$ and $|H_{eq2}(f)|$ for $R_1 = 200\Omega, R_2 = 50\Omega, C_1 = 10\,\text{pF}, C_2 = 2.5\,\text{pF}$.

Fig. 11(a) and (b) compare $|H_{eq1}(f)|$ and $|H_{eq2}(f)|$ obtained using (26) with those from sampled PXF simulations in Spectre, for the 4-path network of Fig. 7, with $f_s = 1\,\text{GHz}$, $R_1 = 200\Omega, R_2 = 50\Omega, C_1 = 200\,\text{pF}, C_2 = 50\,\text{pF}$. Excellent agreement is seen.

IV. Complete Signal-Flow Graph and Operation in the Passive-Mixer and N-Path Filter Modes

Fig. 12 shows the signal-flow graph of the capacitor waveforms of the kernel. It is a generalized version of that used in [16], and results from reasoning as in Section 4 of [16]. The capacitor voltages can be expressed as the sum of two waveforms: $\mathbf{v_{off}}(t)$ that is non-zero when the switches are open, i.e., the time intervals $lT_s \le t < (l+1)T_s - \tau$, and $\mathbf{v_{on}}(t)$, which is non-zero when the switches are closed, i.e., the intervals $(l+1)T_s - \tau \le t < (l+1)T_s$. The sum of paths ⓐ and ⓑ yields $\mathbf{v_{on}}(t)$. $w(t)$ is 1 when ϕ_1 is high and 0 otherwise. Fig. 12 immediately relatable to Fig. 7 of [16], where $\beta, h(t)$ and $(1/RC)h(t)$ are replaced by $e^{\mathbf{A}\tau}, e^{\mathbf{A}t}u(t)$ and $e^{\mathbf{A}t}\mathbf{B}u(t)$ respectively. The signal-flow can be simplified for operation in the passive-mixer and N-path filter modes, as discussed below.

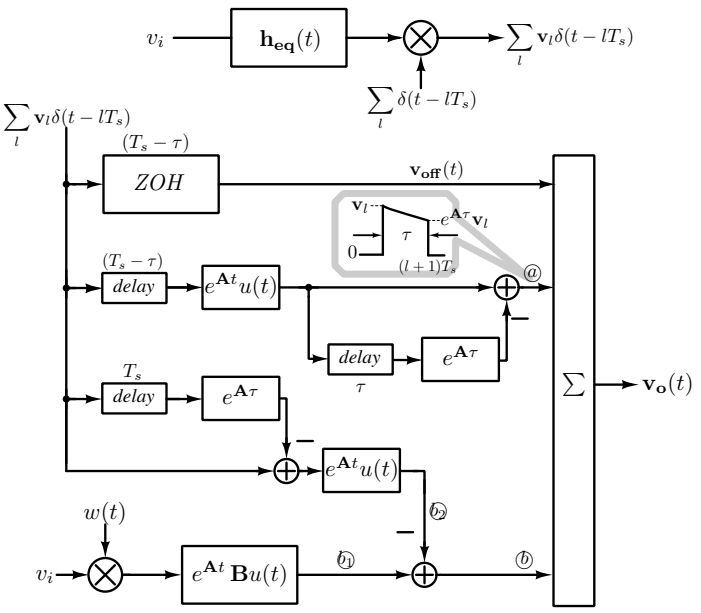

Fig. 12. Signal flow graph relating the input and the complete output of the switched-RC kernel.

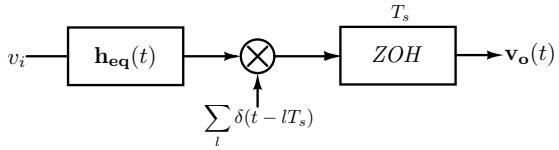

Fig. 13. Simplified signal-flow graph in the passive-mixer mode.

A. Passive-Mixer Mode

In the passive-mixer (P-M) mode, $f_{in} \approx f_s + \Delta f$. Further, the input frequency is much higher than the bandwidth of the prototype filter. Under these circumstances, the output voltage of Fig. 12 can then be simplified by recognizing the following. The output of path ⓑ is very small, since the input frequency is very large in relation to the bandwidth of the filter. Further, $e^{\mathbf{A}t}u(t)$ is almost a unit-step function, since all time-constants are much larger than T_s. As a result, $e^{\mathbf{A}t}u(t)$ and the subsequent block in path ⓐ can be approximated by a ZOH, with initial delay of $(T_s - \tau)$ and width τ. Together with the ZOH that models $\mathbf{v_{off}}(t)$, $\mathbf{v_o}(t)$ can be approximated as a single ZOH with width T_s. Fig. 13 shows the simplified model of the kernel in the P-M mode. Thus, as concluded in [13] and [16] for the simple RC case, the performance in the P-M mode is dependent mostly on the sampled capacitor voltages.

B. N-path Filter Mode:

An important application of the switched-RC network is its use as an N-path filter. Our example of Fig. 7 (where $N = 4$) is based on a second-order kernel. The switches are controlled by non-overlapping clocks of width $\tau = T_s/N$. In N-path operation, the voltage waveforms at v_{x1} and v_{x2} are relevant. They depend on $\mathbf{v_{on}}(t)$ of the kernel. Referring to Fig. 12, this is seen to be the sum of paths ⓐ and ⓑ. Further, notice that the contributions of the paths with gain $e^{\mathbf{A}\tau}$ cancel at the output. Thus, $\mathbf{v_{on}}(t)$ can be simplified as shown in Fig. 14.

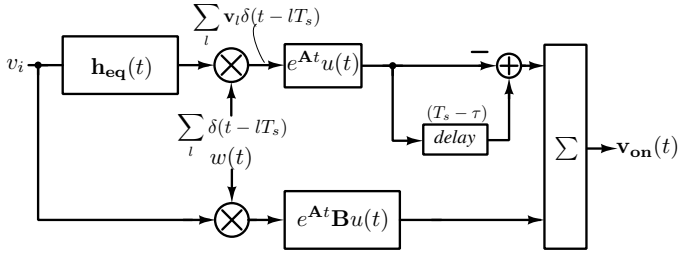

Fig. 14. Signal-flow graph for operation as an N-path filter.

The zeroth order harmonic transfer functions of the kernel can be found from Fig. 14 by using $v_i(t) = e^{j2\pi ft}$, and determining the components $\mathbf{v_{on}}(t)$ at the frequency f. The corresponding transfer function $\mathbf{H}_0(f)$ of the N-path filter is N times that of the kernel. Analysis of the signal-flow graph of Fig. 14 shows that

$$\begin{aligned}\mathbf{H}_0(f) &= -\frac{N}{T_s}(j2\pi f\mathbf{I}-\mathbf{A})^{-1}\mathbf{H_{eq}}(f)(1-e^{-j2\pi f(T_s-\tau)}) \\ &\quad +(j2\pi f\mathbf{I}-\mathbf{A})^{-1}\mathbf{B}. \qquad (27)\end{aligned}$$

The expression above makes sense due to the following. The input, after being filtered by $\mathbf{H_{eq}}(f)$, is sampled yielding a modulated impulse train. The frequency component of this at f, when filtered by the time-invariant transfer function that comprises the upper arm of the signal-flow graph of Fig. 14, and multiplied by N yields the first term of $\mathbf{H}_0(f)$. The lower arm, whose zeroth order transfer function is $(1/N)(j2\pi f\mathbf{I}-\mathbf{A})^{-1}\mathbf{B}$, yields the second term. As expected, (27) reduces to (18) in [16] when a first-order RC lowpass prototype is used. Fig. 15 compares the analytically calculated zeroth order HTFs for the voltages across the capacitors, with those obtained from simulation. Excellent agreement is seen.

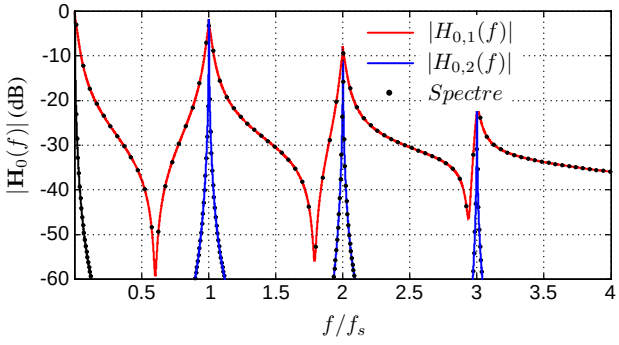

Fig. 15. Analytical and simulated harmonic transfer functions $H_{0,1}$ and $H_{0,2}$ in the N-path filter mode, for the network of Fig. 7. $R_1 = 200\Omega, R_2 = 50\Omega, C_1 = 10\,\text{pF}, C_2 = 2.5\,\text{pF}$.

Thanks to N-path operation, only the N^{th} order HTFs (and their multiples) are relevant. Since the width of $w(t)$ is T_s/N, its N^{th} order Fourier coefficients are all zero. Thus, the lower path in Fig. 14 does not contribute to higher order HTFs. If v_i is $e^{j2\pi f_i t}$, the output at a frequency $(f_i + kNf_s) \equiv f_o$ is given by $\mathbf{H}_{kN}(f_i)e^{j2\pi f_o t}$ for $k \neq 0$, where

$$\mathbf{H}_{kN}(f_i) = -\frac{N}{T_s}(j2\pi f_o\mathbf{I}-\mathbf{A})^{-1}\mathbf{H_{eq}}(f_i)(1-e^{-j2\pi f_o(T_s-\tau)}). \qquad (28)$$

Fig. 16 compares the analytically calculated $\mathbf{H}_{-4}$ for the voltages across the capacitors, with those obtained from simulation. From the discussion above, we see that the sampled capacitor voltages play a crucial role in determining the downconversion of signal from around multiples of Nf_s into the signal band.

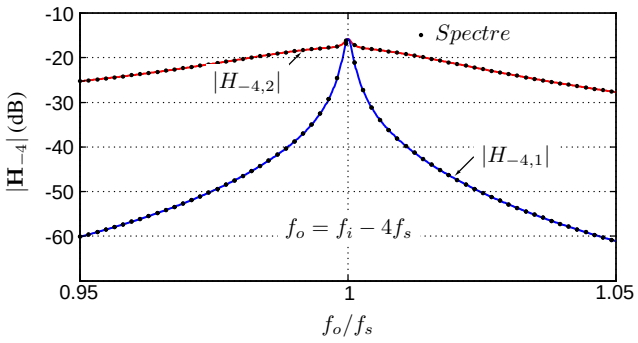

Fig. 16. Analytical and simulated fourth order harmonic transfer functions in the N-path filter mode, for the network of Fig. 7. $R_1 = 200\Omega, R_2 = 50\Omega, C_1 = 10\,\text{pF}, C_2 = 2.5\,\text{pF}$.

V. Analysis of an N-Path Mixer-First Receiver with Fourth-Order RF Filtering

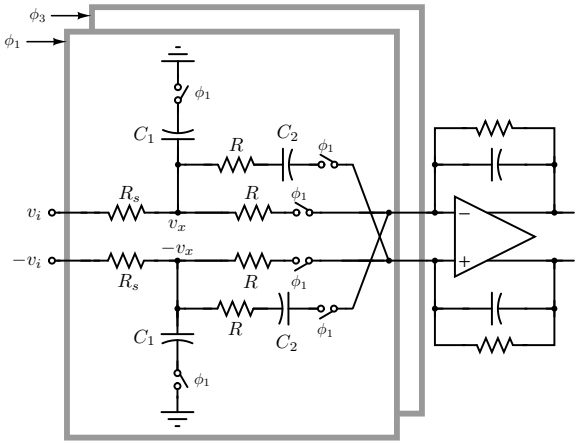

Fig. 17. The in-phase portion of the 4-path mixer-first receiver of Lien et. al. [18].

One of the motivations for the generalized development in this paper was the work in [18], which combines N-path filtering and N-path mixing using a second-order switch-RC network. The simplified schematic of the in-phase path of the receiver is shown in Fig. 17. The OTA is assumed to be ideal. The intuition behind the operation of this circuit is as follows. The switched C_1 bank behaves like a parallel LC tank – as a result, the voltage at node v_x has a bandpass response centered at f_s. The roll-off of the bandpass characteristic around f_s is of first order.

v_x is down-converted to a baseband current by the switched resistor feeding into the virtual ground of the OTA. The switched-C_2 path behaves like a notch filter centered at f_s. The currents in these paths are subtracted at the virtual ground of the OTA. A better understanding of the operation of the filter can be gained by analyzing the single-ended equivalent of the input circuit, shown in Fig. 18(a). v_x is bandpass filtered due to the switched-C_1.

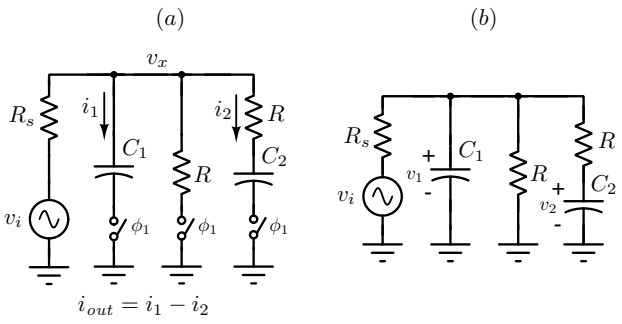

Fig. 18. (a) Single-ended portion of the input circuit of Fig. 17. (b) The lowpass prototype on which the N-path circuit is based.

i_1 is the down-converted version of v_x. It not only consists of current due to the desired signal, but also that due to out-of-band interferers, which have been (somewhat) attenuated by bandpass filtering at v_x. To attenuate out-of-band interference even more before entering active amplifier stages (which are lot less linear), another stage of passive N-path filtering is desirable. This is possible by subtracting the current due to out-of-band components by processing v_x through a notch filter formed by R in series with the switched-C_2 path. i_2, therefore, consists predominantly of current due to out-of-band interferers [18]. As a result, $(i_1 - i_2)$ is largely free of interferers, resulting in enhanced receiver linearity. Thanks to subtracting the current through the notch filter, second-order filtering around f_s is obtained; one order of filtering due to the switched C_1, and another order due to the subtraction of the notch filter output.

The output of interest is $(i_1 - i_2)$. From Fig. 18(a) and using $G = 1/R$, we see that

$$i_1(t) = G v_{1,on}(t) \quad , \quad i_2(t) = G(v_{1,on}(t) - v_{2,on}(t))$$

which results in $i_1(t) - i_2(t) = G v_{2,on}(t)$. Thus, subtracting i_2 from i_1 is equivalent to sensing the voltage across C_2 (and multiplied by G) in the phase when the switches are on. If the feedback resistor in the opamp (Fig. 17) is $R = 1/G$, the output of the kernel is simply the "on=phase" voltage waveform across C_2.

Perhaps an even simpler way of understanding the circuit operation is to consider the lowpass prototype on which the N-path filter is based, as shown in Fig. 18(b). Straightforward circuit analysis shows that

$$\frac{V_2(s)}{V_i(s)} = \frac{R/(R+R_s)}{1 + sR\left(C_2 + (C_1+C_2)\frac{R_s}{R_s+R}\right) + s^2 C_1 C_2 R^2 \frac{R_s}{R_s+R}}.$$

Since the prototype transfer function is a second-order lowpass filter, it follows that the N-path filter of Fig. 18(a) will have a fourth-order bandpass response centered around f_s, with a second-order roll-off around f_s. Since the passive prototype consists only of resistors and capacitors, its poles lie on the negative-real axis. As a result, the transfer function can only achieve a limited "sharpness", and the same limitation applies to the bandpass characteristic of the N-path structure.

Referring to Fig. 18(a), we are interested in determining v_2 when the switch is on, since $(i_1(t) - i_2(t)) = G v_{2,on}(t)$. Inspection of Fig. 18(b) yields

$$\mathbf{A} = -\begin{bmatrix} C_1 & 0 \\ 0 & C_2 \end{bmatrix}^{-1} \begin{bmatrix} (G_s + 2G) & -G \\ -G & G \end{bmatrix}, \mathbf{B} = \begin{bmatrix} G_s/C_1 \\ 0 \end{bmatrix}.$$

Since we are interested in the operation of Fig. 17 as a down-conversion mixer, the (-1)$^{\text{th}}$ harmonic transfer function needs to be determined. Let $v_i = e^{j2\pi f_i t}$: then, the output frequency of interest is $f_o \equiv f_i - f_s$. We use the signal-flow graph of Fig. 14 to determine $\mathbf{v_{on}}$. The analysis proceeds in much the same manner as that used to derive (27). The desired HTF is given by

$$\mathbf{H}_{-1}(f_i) = \frac{1}{T_s}\mathbf{H_{eq}}(f_i)\ (j2\pi f_o \mathbf{I} - \mathbf{A})^{-1}\ (e^{-j2\pi f_o(T_s-\tau)} - 1) + \underbrace{\frac{1}{N}\text{sinc}\left(\frac{1}{N}\right) e^{-j\frac{\pi}{N}}}_{\substack{\text{Coefficient of } e^{-j2\pi f_s t} \\ \text{in the Fourier} \\ \text{expansion of } w(t)}} (j2\pi f_o \mathbf{I} - \mathbf{A})^{-1}\mathbf{B}. \quad (29)$$

Note that the lower path in the signal-flow graph of Fig. 14 yields the second term in the equation above.

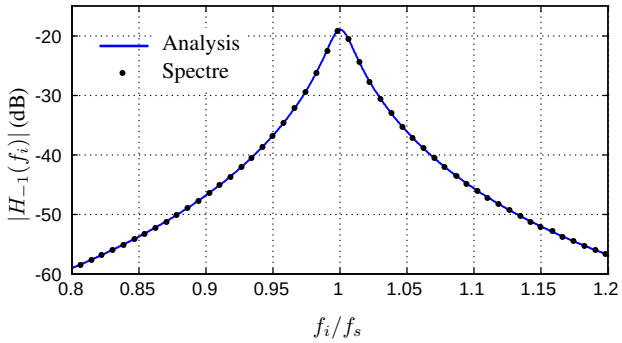

Fig. 19. Simulated and calculated downconversion gain of Lien's circuit, with $N = 4$, $C_1 = C_2 = 50\,\text{pF}$, $R = R_s = 50\,\Omega$.

Fig. 19 compares the simulated and calculated downconversion gain of Lien's circuit, with $N = 4$, $C_1 = C_2 = 50\,\text{pF}$, $R = R_s = 50\,\Omega$. Excellent agreement is seen.

Fig. 20 shows a log-log plot of $|H_{-1}(f_i)|$ plotted as a function of the output frequency f_o. The frequency-scaled response of the lowpass prototype is also shown for comparison. We see that for "low" frequencies, the downconversion gain follows that of the lowpass prototype. This makes sense, since the sampled voltage on the capacitor dominates the direct contribution of the input at low frequencies.

VI. Conclusions

We developed a systematic analysis of switch-RC N-path passive-mixers and filters. Our work is able to exactly predict frequency conversion effects even in high-order filters. Our techniques also yield simple expressions, immediately relatable to those encountered during the analysis of the first-order switched-RC network. This is possible thanks to the use of the adjoint impulse response method, and the state-space formulation to describe the prototype lowpass network. Simplified models for operation in the passive-mixer and N-path filter modes are given. Finally, we applied our theory to a recently reported mixer-first receiver. Excellent agreement was seen with simulation.

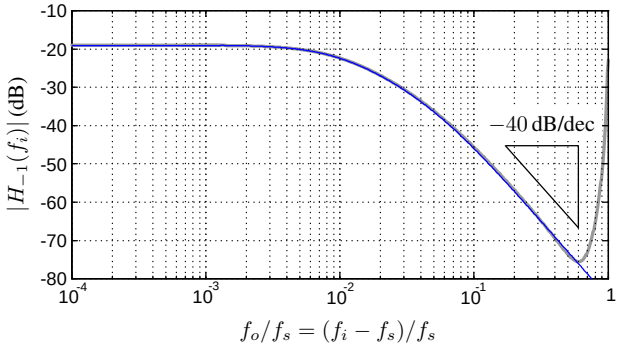

Fig. 20. Log-log plot of $|H_{-1}(f_i)|$ plotted as a function of f_o. The transfer function of the frequency-scaled lowpass prototype is also shown for comparison. $N = 4$, $C_1 = C_2 = 50\,\text{pF}$, $R = R_s = 50\,\Omega$.

APPENDIX

The MNA equations for the network can be written as

$$\mathbf{C}\dot{\mathbf{v}} + \mathbf{G}\mathbf{v} = \mathbf{J}v_i \tag{30}$$

where $\mathbf{C}$ and $\mathbf{G}$ are the capacitance and conductance matrices. $\mathbf{J}$ denotes the excitation matrix. $\mathbf{C}$ is a diagonal matrix, and as the network does not contain controlled sources, $\mathbf{G}$ is symmetric. The equation above can be recast in state-space form as

$$\dot{\mathbf{v}} = \underbrace{-\mathbf{C}^{-1}\mathbf{G}}_{\mathbf{A}}\mathbf{v} + \underbrace{\mathbf{C}^{-1}\mathbf{J}}_{\mathbf{B}}v_i \tag{31}$$

In our second-order example (which is easily generalized),

$$\mathbf{C} = \begin{bmatrix} C_1 & 0 \\ 0 & C_2 \end{bmatrix} \text{ and } \mathbf{C}^{-1} = \begin{bmatrix} \frac{1}{C_1} & 0 \\ 0 & \frac{1}{C_2} \end{bmatrix}. \tag{32}$$

Since $\mathbf{G}$ and $\mathbf{C}$ are symmetric, $\mathbf{A}^T = -\mathbf{G}\mathbf{C}^{-1}$. The term $\mathbf{C}^{-1}e^{\mathbf{A}^T\tau}\mathbf{C}$ in (21) can be simplified by expanding $e^{\mathbf{A}^T\tau}$ in a Taylor series as follows.

$$\begin{aligned} & \mathbf{C}^{-1}e^{\mathbf{A}^T\tau}\mathbf{C} \\ = \; & \mathbf{C}^{-1}(\mathbf{I} - \mathbf{G}\mathbf{C}^{-1}\tau + \frac{1}{2}\mathbf{G}\mathbf{C}^{-1}\mathbf{G}\mathbf{C}^{-1}\tau^2 - \cdots)\mathbf{C} \\ = \; & \mathbf{I} - \mathbf{C}^{-1}\mathbf{G}\tau + \frac{1}{2}\mathbf{C}^{-1}\mathbf{G}\mathbf{C}^{-1}\mathbf{G}\tau^2 - \cdots \\ = \; & e^{-\mathbf{C}^{-1}\mathbf{G}\tau} = e^{\mathbf{A}\tau}. \end{aligned} \tag{33}$$

REFERENCES

[1] M. Van Valkenburg, *Analog Filter Design*. Holt, Rinehart, and Winston, 1982.

[2] M. C. Soer, E. A. Klumperink, P.-T. De Boer, F. E. Van Vliet, and B. Nauta, "Unified frequency-domain analysis of switched-series-*RC* passive mixers and samplers," *IEEE Transactions on Circuits and Systems I: Regular Papers*, vol. 57, no. 10, pp. 2618–2631, 2010.

[3] C. Andrews and A. C. Molnar, "A passive mixer-first receiver with digitally controlled and widely tunable RF interface," *IEEE Journal of solid-state circuits*, vol. 45, no. 12, pp. 2696–2708, 2010.

[4] ——, "Implications of passive mixer transparency for impedance matching and noise figure in passive mixer-first receivers," *IEEE Transactions on Circuits and Systems I: Regular Papers*, vol. 57, no. 12, pp. 3092–3103, 2010.

[5] A. Mirzaei, H. Darabi, and D. Murphy, "Architectural evolution of integrated M-phase high-Q bandpass filters," *IEEE Transactions on Circuits and Systems I: Regular Papers*, vol. 59, no. 1, pp. 52–65, 2012.

[6] A. Ghaffari, E. A. Klumperink, M. C. Soer, and B. Nauta, "Tunable high-Q N-path band-pass filters: Modeling and verification," *IEEE Journal of Solid-State Circuits*, vol. 46, no. 5, pp. 998–1010, 2011.

[7] A. Ghaffari, E. A. Klumperink, and B. Nauta, "Tunable N-path notch filters for blocker suppression: Modeling and verification," *IEEE Journal of Solid-State Circuits*, vol. 48, no. 6, pp. 1370–1382, 2013.

[8] L. Duipmans, R. E. Struiksma, E. A. Klumperink, B. Nauta, and F. E. van Vliet, "Analysis of the signal transfer and folding in n-path filters with a series inductance," *IEEE Transactions on Circuits and Systems I: Regular Papers*, vol. 62, no. 1, pp. 263–272, 2015.

[9] M. Darvishi, R. van der Zee, E. A. Klumperink, and B. Nauta, "Widely tunable 4th order switched G_m-C band-pass filter based on N-path filters," *IEEE Journal of Solid-State Circuits*, vol. 47, no. 12, pp. 3105–3119, 2012.

[10] M. Darvishi, R. van der Zee, and B. Nauta, "Design of active N-path filters," *IEEE Journal of Solid-State Circuits*, vol. 48, no. 12, pp. 2962–2976, 2013.

[11] Z. Lin, P. I. Mak, and R. P. Martins, "Analysis and modeling of a gain-boosted N-path switched-capacitor bandpass filter," *IEEE Transactions on Circuits and Systems I: Regular Papers*, vol. 61, no. 9, pp. 2560–2568, 2014.

[12] N. Reiskarimian, J. Zhou, T.-H. Chuang, and H. Krishnaswamy, "Analysis and design of two-port N-path bandpass filters with embedded phase shifting," *IEEE Transactions on Circuits and Systems II: Express Briefs*, vol. 63, no. 8, pp. 728–732, 2016.

[13] T. Iizuka and A. A. Abidi, "FET-RC Circuits: A unified treatment - Part I: Signal transfer characteristics of a single-path," *IEEE Transactions on Circuits and Systems I: Regular Papers*, vol. 63, no. 9, pp. 1325–1336, 2016.

[14] ——, "FET-RC Circuits: A unified treatment - Part II: Extension to multi-paths, noise figure, and driving-point impedance," *IEEE Transactions on Circuits and Systems I: Regular Papers*, vol. 63, no. 9, pp. 1337–1348, 2016.

[15] E. S. Atalla, F. Zhang, P. T. Balsara, A. Bellaouar, S. Ba, and K. Kiasaleh, "Time-domain analysis of passive mixer impedance: A switched-capacitor approach," *IEEE Transactions on Circuits and Systems I: Regular Papers*, vol. 64, no. 2, pp. 347–359, 2017.

[16] S. Pavan and E. Klumperink, "Simplified unified analysis of switched-RC samplers, mixers and N-path filters using the adjoint network," *IEEE Transactions on Circuits and Systems I: Regular Papers*, vol. 64, no. 10, pp. 2714–2725, 2017.

[17] A. Mirzaei and H. Darabi, "Analysis of imperfections on performance of 4-phase passive-mixer-based high-Q bandpass filters in SAW-less receivers," *IEEE Transactions on Circuits and Systems I: Regular Papers*, vol. 58, no. 5, pp. 879–892, 2011.

[18] Y. Lien, E. Klumperink, B. Tenbroek, J. Strange, and B. Nauta, "A high-linearity CMOS receiver achieving +44 dBm IIP3 and +13 dBm 1 dB for SAW-less LTE radio," in *Proc. of the IEEE International Solid-State Circuits Conference (ISSCC),*. IEEE, 2017, pp. 412–413.

[19] T. Strom and S. Signell, "Analysis of periodically switched linear circuits," *IEEE Transactions on Circuits and Systems*, vol. 24, no. 10, pp. 531–541, 1977.

[20] A. Fettweis, "Theory of stop-go N-path filters," *Archiv Fur Elektronik Und Ubertragungstechnik*, vol. 25, no. 4, p. 173, 1971.

[21] S. Pavan and R. S. Rajan, "Interreciprocity in linear periodically time-varying networks with sampled outputs," *IEEE Transactions on Circuits and Systems II: Express Briefs*, vol. 61, no. 9, pp. 686–690, 2014.

[22] S. Pavan and E. Klumperink, "Analysis of the effect of source capacitance and inductance on n-path mixers and filters," *IEEE Transactions on Circuits and Systems I: Regular Papers*, vol. 65, p. To appear, 2018.

[23] A. Fettweis and H. Wupper, "A solution to the balancing problem in N-path filters," *IEEE Transactions on Circuit Theory*, vol. 18, no. 3, pp. 403–405, 1971.

[24] H. Patangia and M. Blostein, "A digitally controlled tunable N-path filter," *IEEE Transactions on Circuits and Systems*, vol. 25, no. 3, pp. 135–144, 1978.

[25] C.-T. Chen, *Linear System Theory and Design*. Oxford University Press, Inc., 1995.

[26] L. O. Chua, C. A. Desoer, and E. S. Kuh, *Linear and Nonlinear Circuits*. McGraw-Hill College, 1987.

Shanthi Pavan obtained the B.Tech degree in Electronics and Communication Engg from the Indian Institute of Technology, Madras in 1995 and the M.S and Sc.D degrees from Columbia University, New York in 1997 and 1999 respectively. From 1997 to 2000, he was with Texas Instruments in Warren, New Jersey, where he worked on high speed analog filters and data converters. From 2000 to June 2002, he worked on microwave ICs for data communication at Bigbear Networks in Sunnyvale, California. Since July 2002, he has been with the Indian Institute of Technology-Madras, where he is now a Professor of Electrical Engineering. His research interests are in the areas of high speed analog circuit design and signal processing.

Dr. Pavan is the recipient of the IEEE Circuits and Systems Society Darlington Best Paper Award (2009), the Shanti Swarup Bhatnagar Award (2012) and the Swarnajayanthi Fellowship (2009) (from the Government of India), the Mid-career Research Excellence Award and the Young Faculty Recognition Award from IIT Madras (for excellence in teaching), the Technomentor Award from the India Semiconductor Association and the Young Engineer Award from the Indian National Academy of Engineering (2006). He is the author of *Understanding Delta-Sigma Data Converters (second edition), with Richard Schreier and Gabor Temes)*. Dr. Pavan has served as the Editor-in-Chief of the *IEEE Transactions on Circuits and Systems: Part I - Regular Papers*, and on the editorial boards of both parts of the *IEEE Transactions on Circuits and Systems*. He has served on the technical program committee of the International Solid State Circuits Conference, and been a Distinguished Lecturer of the Solid-State Circuits Society. He is a fellow of the Indian National Academy of Engineering.

Eric Klumperink was born on April 4th, 1960, in Lichtenvoorde, The Netherlands. He received the B.Sc. degree from HTS, Enschede (1982), worked in industry on digital hardware and software, and then joined the University of Twente in 1984, shifting focus to analog CMOS circuit research. This resulted in several publications and his Ph.D. thesis "Transconductance Based CMOS Circuits" (1997). In 1998, Eric started as Assistant Professor at the IC-Design Laboratory in Twente and shifted research focus to RF CMOS circuits (e.g. sabbatical at the Ruhr Universitaet in Bochum, Germany). Since 2006, he is an Associate Professor, teaching Analog & RF IC Electronics and guiding PhD and MSc projects related to RF CMOS circuit design with focus on Software Defined Radio, Cognitive Radio and Beamforming. He served as an Associate Editor for the IEEE TCAS-II (2006-2007), IEEE TCAS-I (2008-2009) and the IEEE JSSC (2010-2014), as IEEE SSC Distinguished Lecturer (2014/2015), and as member of the technical program committees of ISSCC (2011-2016) and the IEEE RFIC Symposium (2011-..). He holds several patents, authored and co-authored 150+ internationally refereed journal and conference papers, and was recognized as 20+ ISSCC paper contributor over 1954-2013. He is a co-recipient of the ISSCC 2002 and the ISSCC 2009 "Van Vessem Outstanding Paper Award".